

Effect of Flexibility and Nanotriboelectrification on the Dynamic Reversibility of Water Intrusion into Nanopores: Pressure-Transmitting Fluid with Frequency-Dependent Dissipation Capability

Alexander Lowe,[†] Nikolay Tsyryn,[‡] Mirosław Chorażewski,[†] Paweł Zajdel,[§] Michał Mierzwa,^{§,||} Juscelino B. Leão,[⊥] Markus Bleuel,^{⊥,#} Tong Feng,[¶] Dong Luo,[∇] Mian Li,[¶] Dan Li,[∇] Victor Stoudenets,[‡] Sebastian Pawlus,^{§,||} Abdessamad Faik,[○] and Yaroslav Grosu^{*,○}

[†]Institute of Chemistry, University of Silesia, Szkolna 9, 40-006 Katowice, Poland

[‡]Laboratory of Thermomolecular Energetics, National Technical University of Ukraine “Igor Sikorsky Kyiv Polytechnic Institute”, Pr. Peremogy 37, 03056 Kyiv, Ukraine

[§]Institute of Physics, University of Silesia, 75 Pulku Piechoty 1, 41-500 Chorzow, Poland

^{||}Silesian Center for Education and Interdisciplinary Research, University of Silesia, 75 Pulku Piechoty 1A, 41-500 Chorzow, Poland

[⊥]NIST Center for Neutron Research, National Institute of Standards and Technology, Gaithersburg, Maryland 20899, United States

[#]Department of Materials Science and Engineering, University of Maryland, College Park, Maryland 20742-2115, United States

[¶]Department of Chemistry, Shantou University, Shantou, Guangdong 515063, China

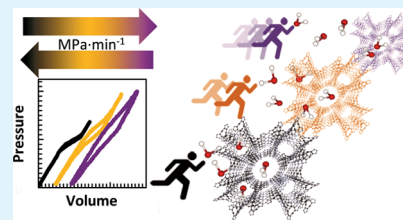
[∇]College of Chemistry and Materials Science, Jinan University, 510632 Guangzhou, China

[○]CIC Energigune, Albert Einstein 48, Miñano, Álava 01510, Spain

Supporting Information

ABSTRACT: In this article, the effect of a porous material's flexibility on the dynamic reversibility of a nonwetting liquid intrusion was explored experimentally. For this purpose, high-pressure water intrusion together with high-pressure in situ small-angle neutron scattering were applied for superhydrophobic grafted silica and two metal–organic frameworks (MOFs) with different flexibility [ZIF-8 and Cu₂(tebpz) (tebpz = 3,3',5,5'-tetraethyl-4,4'-bipyrazolate)]. These results established the relation between the pressurization rate, water intrusion–extrusion hysteresis, and porous materials' flexibility. It was demonstrated that the dynamic hysteresis of water intrusion into superhydrophobic nanopores can be controlled by the flexibility of a porous material. This opens a new area of applications for flexible MOFs, namely, a smart pressure-transmitting fluid, capable of dissipating undesired vibrations depending on their frequency. Finally, nanotriboelectric experiments were conducted and the results showed that a porous material's topology is important for electricity generation while not affecting the dynamic hysteresis at any speed.

KEYWORDS: flexibility, porous material, MOF, anti-vibration protection, smart working body, energy storage/dissipation



1. INTRODUCTION

With an exponentially increasing global population and corresponding energy demand,¹ new methods must be created to store and transform renewable energy. One of the most utilized mechanisms, which is currently under study is the ability to convert mechanical energy, with the particular application to energy generators for electricity.² The current generation of mechanical energy storage technologies which are in use includes the flywheel, compressed air, and pumped hydroenergy.³ While useful, they are large and bulky, require a lot of space, and have limited applications in a confined area. To overcome these challenges new technologies and materials must be developed, which can be miniaturized and efficiently transform or dissipate energy.

The reversible intrusion of nonwetting liquids into nanoporous solids is an attractive process for energy applications. Historically, the pioneering studies were done by Eroshenko⁴ with Fadeev,^{5–8} Regis, Soulard, Patarin,^{9,10} and Coiffard,^{11–13} for this kind of mechanical energy storage/dissipation. Since then, researchers have investigated many different combinations of nonwetting liquids and solutions with porous solids. The properties of these combined materials should produce a system, which is chemically inert, durable over a wide range of temperature and pressure conditions, efficient in converting energy, possess a large energy density, and economically viable.

Received: August 6, 2019

Accepted: October 2, 2019

Published: October 2, 2019

A number of systems have been studied which involve grafted silica^{8,11–19} or aluminosilicate²⁰ based porous materials with either water or aqueous electrolyte solutions as the nonwetting liquids. Some studies have included the examination of the change in lattice parameters and unit cell volume of siliceous zeolites and pore-filling process with water,²¹ while simultaneously studying the structure of confined water. Recently the range of porous materials was extended to metal–organic frameworks (MOFs).^{22–32}

Intrusion–extrusion of water into–from nanopores is a complex process, which can involve many different physical phenomena, such as capillarity, bubble nucleation,^{33–35} triboelectrification,³⁶ viscosity,³⁷ and osmotic pressure.³⁸ The breadth of work dedicated to this topic is quite large, but the phenomena which govern the intrusion–extrusion pressure hysteresis are not completely understood. What is clear is how to exploit this hysteresis to make a useful system composed of nonwetting liquids and porous solids. These systems belong to three different categories. The first category is the molecular bumper where the intrusion of liquid is observed without corresponding extrusion.³⁹ The second is a molecular shock-absorber where cyclic intrusion and extrusion is absorbed with a large difference between the intrusion pressures and extrusion pressure.^{8,11,12,14–19,23,24} The final category is a molecular spring where the differences between intrusion and extrusion pressures are small or nonexistent thus creating an ideal reversible cycle.²⁶ Therefore, intrusion–extrusion pressure hysteresis is the parameter determining the application target of similar heterogeneous lyophobic systems.

ZIF-7 and ZIF-8 systems are well-known flexible systems^{30,31} which have a gate-type mechanism.^{28,40} The study of these systems shows that liquid intrusion can be facilitated, with respect to ZIF-7, by this gating mechanism and is dependent on the rate of intrusion and rate of relaxation of the solid material.⁴⁰ The disadvantage is that this material is unstable, so it degrades after long periods of water immersion. On the other hand, ZIF-8 is stable in water and can be repeatedly exposed to continuous intrusion extrusion cycles with very little changes in pressure–volume (PV) cycles at ambient temperatures.^{28,31}

In this study, a new parameter is introduced for the dynamic intrusion–extrusion hysteresis, which is the compressibility of flexible porous materials. The aim of this work is to investigate the dynamic aspects of intrusion–extrusion hysteresis by focusing on the role of the framework flexibility of porous materials under high-pressure cycling conditions. These experiments are conducted with compression/decompression speeds ranging from 0.1 MPa min^{−1} to 9 GPa min^{−1} using unique high-pressure equipment. The systems being studied are suspensions which comprise water, as the nonwetting liquid and a single solid nanoporous material. In total three different suspensions are investigated. The first includes a grafted silica gel. For the second and third systems the solids are MOFs, which display different pore topologies. Each of these suspension systems have the ability to recover its original state after the applied stress is removed. Remarkably, it was found that materials with prominent flexibility behave as either a molecular spring or molecular bumper depending on the velocity of impact. These systems can be named as “smart suspension”. A further study using adapted dielectric spectroscopy equipment was conducted to determine if triboelectrification phenomena contribute to the dynamic hysteresis. In situ high-pressure small-angle neutrons scattering

(vSANS) experiments were conducted to gain insight into the flexibility phenomena during the intrusion process.

Based on this knowledge, a new concept is proposed of a smart suspension system with frequency-enabled energy storage and/or dissipation capability. What is being proposed is that the material with considerable flexibility is capable of storing mechanical energy at low frequencies while dissipating-adsorbing energy at high frequencies of compression/decompression cycles. Conceptually, this is a mechanical analogy to a low-pass filter. Such systems have the potential to serve as a smart pressure-transmitting fluid, which is capable of dissipating undesirable vibrations during its operation.

2. MATERIALS AND METHODS

2.1. Materials. Three porous materials were chosen for this study. The first is a commercially prepared mesoporous silica gel SymmetryPrep C8 purchased from WATERS and known as WC8. The material is composed of 7 μm silica granules grafted with octylsilanes with a density of 2.1 groups nm^{−2} according to the supplier. The second material is the MOF ZIF-8 which was purchased from Sigma-Aldrich as Basolite Z1200, CAS# 59061-53-9. The pore orifice size of ZIF-8 is 0.34 nm with a surface area of 1800 m² g^{−1}. The third material is Cu₂(tebpz) MOF (tebpz = 3,3',5,5'tetraethyl-4,4'-bipyrazolate) which was synthesized for these experiments according to the procedure of Wang et al.,⁴¹ and was tested for molecular spring application by Grosu et al.²⁶ Cu₂(tebpz) presents three sets of highly ordered cylindrical pores of (1) 0.46 × 0.47 nm²; (2) 0.65 × 0.65 nm²; and (3) 0.63 × 1.32 nm² with a pore volume of 0.53 cm³ g^{−1}.⁴¹ Distilled and deionized water was used as the nonwetting liquid for PV-isotherm experiments. For the in situ small-angle neutron scattering (vSANS) heavy water of 99.9% (D₂O) was used for the compression/decompression cycles. It was purchased from Cambridge Isotope Laboratories Inc.

2.2. Methods. **2.2.1. Equipment for Dynamic PV-Isotherms.** The PV-isotherms were measured at a temperature of 295 K using three different sets of equipment. For the experiments which were conducted using the pressurization rate, *R*, within the range of 0.1–1 MPa min^{−1} a PVT-scanning transiometer, constructed by BGR-Tech, was used at the University of Silesia in Katowice.^{42,43} The liquid suspension samples were prepared by first weighing the solid into a Teflon capsule then submerging it into water. Negative relative pressure was applied to evacuate the gas from the capsule creating the suspension. The Teflon vessel was then placed into a calorimetric vessel where the sample was subject to a minimum of 3 pressurization cycles to ensure repeatability. For the experiments involving the pressurization rate of 10 MPa min^{−1}, they were measured using a Pore Master 60 mercury porosimeter from Quantachrome Instruments. The materials, in this case, were outgassed to a pressure of 30 Pa before mixing with water and being sealed within a flexible hermetic Teflon capsule. The suspension system was then placed in the instrument and subject to a minimum of 10 pressurization cycles to ensure repeatability. The largest pressurization rates of 100–9000 MPa min^{−1} were measured with the PVT-stand developed at the National Technical University of Ukraine “Igor Sikorsky Kyiv Polytechnic Institute” and are described in the articles of Eroshenko et al.^{5,7,8,10} Because of different pressure-transmitting fluids and their different quantity in the hydraulic line for each of the instruments, the PV-isotherms were adjusted following the equation, in order to eliminate the effect of pressure-transmitting fluid compressibility

$$\Delta v = \Delta v_{\text{recorded}} - (\alpha \cdot P + \beta)$$

The values of $\Delta v_{\text{recorded}}$ (cm³ g^{−1}) are the original PV-isotherm data, α and β are constants adjusted to reach a similar volume variation upon compression (similar compressibility) below the intrusion pressure. Scaling with this method preserves the apparent pore volume (intrusion volume) of each PV-isotherm and permits the direct comparison of individual PV-isotherms regardless of equipment used.

2.2.2. Equipment for Electrical Conductivity Experiments. The generation of electrical energy upon the intrusion–extrusion cycle was measured using a high-pressure electric spectroscopy cell, which was adapted to record the electrical current generated during the compression/decompression cycle as was described by Grosu et al.³⁶ with the following modification. A diagram of the cell can be seen in Figure 1. Approximately 50 mg of porous solid was placed on the

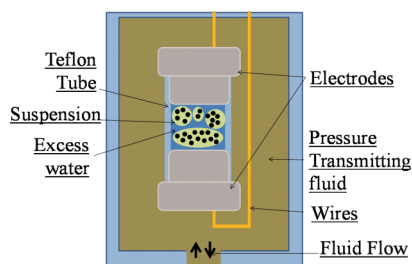


Figure 1. Diagram of a high-pressure electrical cell filled with a suspension of water and nanoporous material.

bottom of a round stainless steel electrodes, with a diameter of 10.5 mm. The electrode is located in tightly fitted Teflon. Deionized water with a resistivity of 18 M Ω was added to the porous material and then the mixture was compressed with a second top electrode. The assembled cell was placed in a vacuum oven to remove any excess air bubbles and create a homogenous suspension. The two electrodes were kept at a distance of 1.6 mm by the enclosing Teflon tube, which hermetically sealed the system. The thickness of the electrodes was 20 mm and their edges have been shaped to ensure tightness. This assisted in sealing the Teflon tube around the electrodes protecting the suspension from exposure to the compression fluid (oil) and preventing the suspension from escaping. No short-circuits were observed during the experiments. A constant voltage of 1 V was applied to the cell while the current was measured between them when varying the pressure in the cell. The compression cycles up to 50 MPa using various compression speeds were conducted at 299 K temperatures. The measurements were performed using modular a DAQ system with separate eight channel input and output voltage cards.

2.2.3. In Situ Small-Angle Neutron Scattering. The vSANS study was carried out at the NIST Center for Neutron Research (Gaithersburg, USA) using the 45 m vSANS instrument. A complete description of the instrument is located at the NCNR WWW site (<http://www.ncnr.nist.gov/>). The neutron wavelength $\lambda = 4.75$ Å was selected using a double reflection pyrolytic graphite monochromator with a spread $\Delta\lambda/\lambda$ of 0.95%. In a He glovebox, the samples were first outgassed, ex situ using a turbomolecular pump at 90 °C down to 10⁻⁶ mbar and then weighed into the vSANS pressure cell (approx 0.5 g of Cu₂(tebpz) or 1 g of ZIF-8) and evacuated again to remove He at room temperature. D₂O was added to the cell then the pressure was applied and dynamically kept constant (within 0.05 MPa) using an ISCO 100HLX syringe pump. A variable offset between the applied pressure and the sensor was less than 0.2 MPa. The temperature was maintained using a heating block within ± 2 K for Cu₂(tebpz) or a glycol–water batch within 0.1 K for ZIF-8. The collected dataset for each pressure includes one scattering run (300 s for Cu₂(tebpz) and 600 s for ZIF-8) with a respective transmission file of 100 s for both materials. The SANS data were reduced using NCNR SANS macros (SANSMacros) and analyzed and visualized using DAVE (DAVE).

3. RESULTS AND DISCUSSION

3.1. Intrusion–Extrusion Cycles and Hysteresis. The PV-isotherms of water mixed with either WC8, ZIF-8, or Cu₂(tebpz) were obtained with increasing pressurization rates as demonstrated in Figure 2. WC8 is a type of rigid silica with an organic grafting, which presents a large hysteresis between

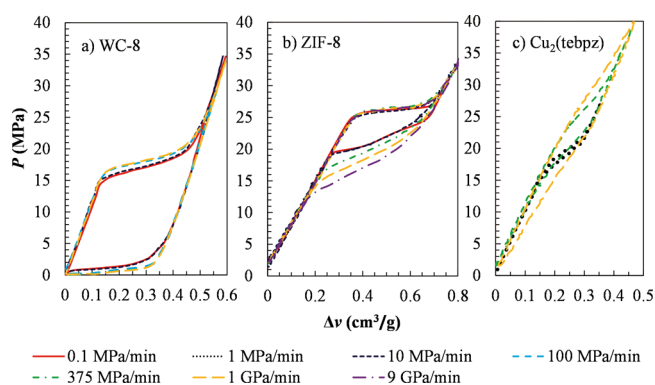


Figure 2. PV-isotherms (295 K) of water with (a) WC8, (b) ZIF-8, and (c) Cu₂(tebpz) using different pressurization rates.

the intrusion and extrusion pressures at the tested pressurization rates, as seen in Figure 2a.

Following the PV-isotherm curve, the pressure rises sharply with a small change in the volume due to systems' limited compressibility until it reaches an intrusion plateau at approximately 17 MPa. At this point, the pores of WC8 begin filling with water. Following the next inflection point, the rise in pressure indicated that WC8 pores have been completely filled and the volume variation is only due to the compressibility of the system. In the decompression experiment, the liquid begins to evacuate the pores at a pressure of 1.5 MPa where the extrusion plateau begins and continues until the pores are emptied. The intrusion pressures (P^{int}) and extrusion pressures (P^{ext}) are defined as the midpoint of the plateau during either the compression or decompression experiments and the values are displayed in Figure 3a,b. The observed pressure hysteresis is calculated with the following equation.

$$H = \left(\frac{P^{\text{int}} - P^{\text{ext}}}{P^{\text{int}}} \right) \times 100\%$$

Figure 3c, as well as Figure 2a, demonstrates that the pressurization rate has a minimum effect on the water intrusion–extrusion pressures, which is simultaneously observed for the hysteresis for WC8.

When placing the ZIF-8 MOF, which is known for its flexibility,^{28,44–46} under the same experimental conditions it is possible to observe similar intrusion behavior, as seen in Figure 2b. As the rate of pressurization increases the PV-isotherms of intrusion do not change significantly. The intrusion pressure of each experiment remains equal at approximately 26.2 MPa even up to pressurization rates of 9 GPa min⁻¹. Contrary to this consistent behavior, the extrusion pressures decrease with the increasing pressurization rate, as seen in Figures 3b and 2b. The change in the hysteresis for this case demonstrates dependence with the rate of depressurization, where the faster rate increases the hysteresis in the cycle as seen in Figures 3c and 2b.

Remarkably, for experiments involving Cu₂(tebpz) the increasing rate of pressurization affects both the intrusion and extrusion pressures significantly, as seen in Figures 3a,b, and 2c. The hysteresis seen in Figure 3c has grown considerably with this increasing rate of pressurization from 1 MPa min⁻¹ to 1 GPa min⁻¹. This fascinating observation is the primary evidence that a nonhysteretic molecular spring can be transformed into a nanobumper by varying the pressuriza-

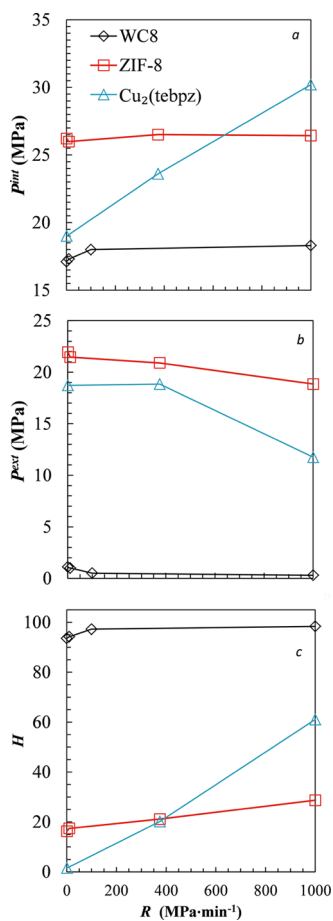


Figure 3. Effect of the pressurization rate, R , on the (a) water intrusion pressure, (b) water extrusion pressure, and (c) hysteresis at 295 K for WC8 (\diamond), ZIF-8 (red \square), and $\text{Cu}_2(\text{tebpz})$ (blue \triangle) systems. The lines running through the data are a visual aide.

tion rate, that is, frequency. This provides a starting point for the development of a smart system, with the capacity of storing/dissipating energy dependence on the pressurization rate. The ability for a material to dissipate mechanical energy is closely related to its hysteresis. An H value of 0 represents a perfect spring, where stored and restored energies are equal, while an H value of 100 represents complete mechanical energy dissipation. The largest hysteresis is observed to belong to WC8, where the hysteretic range is $93 < H < 98$, which has the ability to dissipate a large amount of mechanical energy at any rate of pressurization. For ZIF-8 the hysteresis range is from $17 < H < 33$, meaning that it can restore a modest amount of mechanical energy at low rates of pressurization. While at higher rates of pressurization it behaves more like a shock-absorber. The hysteresis range of $\text{Cu}_2(\text{tebpz})$, which is $1.5 < H < 61$, displays the best ability to adapt to the pressurization rate to store or dissipate mechanical energy, turning from nonhysteretic molecular springs at low compression/decompression rates to an efficient shock-absorber at high compression/decompression rates.

3.2. Effect of Framework Flexibility on the Dynamic Reversibility of Water Intrusion. In order to gain some insights into the mechanism responsible for the drastic difference in the dynamic behavior of water intrusion into nanopores in situ neutron-scattering experiments were performed. In particular, the focus was placed on the evolution

of the unit cell lattice parameters (a , b , c) and the unit cell volume for $\text{Cu}_2(\text{tebpz})$ (seen in Figures S1–S4 and Table S1) and for ZIF-8 (seen in Figures S5–S7 and Table S2) with increasing pressure. These parameters were tracked with the application of increasing pressure on these porous materials using D_2O as the pressure-transmitting fluid. The lattice parameters were calculated from centroids of Gaussian fits to Bragg reflections present in the high- q range of vSANS data. In the case of $\text{Cu}_2(\text{tebpz})$ which crystallizes in an orthorhombic space group, the following procedure was applied.

- 1 The lattice parameter c was calculated by fitting to the (002) reflection in between the range of $0.32\text{--}0.47 \text{ \AA}^{-1}$. This reflection contributes to over 90% of the signal intensity.
- 2 The lattice parameter b was calculated from the lattice parameter c and the centroid of the (022) reflection between the range of $0.46\text{--}0.58 \text{ \AA}^{-1}$.
- 3 The lattice parameter a was calculated from lattice parameters b and c and the centroid of (111) reflection fitted in between the range $0.64\text{--}0.71 \text{ \AA}^{-1}$.

In the case of ZIF-8, the single cubic lattice parameter was calculated from the centroid of the (110) reflection fit in the q -range from 0.46 to 0.80 \AA^{-1} .

For the compressibility analysis, the trends in the data were fit using a linear regression function in their respective pressure regions. All uncertainties of values are statistical and are reported on the $1 - \sigma$ level. For more details see the Supporting Information. These data were used to calculate the isothermal compressibility $\frac{1}{v} \cdot \frac{\partial v}{\partial P}$ for each material as indicated in Table 1. Because no lattice parameters exist for WC8, its

Table 1. Compressibility ($\frac{1}{v} \cdot \frac{\partial v}{\partial P}$) and Dynamic Respond of Water Intrusion Hysteresis (dH/dR) for WC8^b, ZIF-8^c and $\text{Cu}_2(\text{tebpz})$ ^{c,a}

parameter	WC8	ZIF-8	$\text{Cu}_2(\text{tebpz})$
$da/dP (\text{\AA}/\text{MPa}) \times 10^{-4}$		$-7.5(6)$	$-16(4)$
$db/dP (\text{\AA}/\text{MPa}) \times 10^{-4}$			$2(2)$
$dc/dP (\text{\AA}/\text{MPa}) \times 10^{-4}$			$-60(30)$
$\frac{1}{v} \cdot \frac{\partial v}{\partial P} (\text{MPa}^{-1}) \times 10^{-4}$	$-0.36(24)$	$-1.31(4)$	$-3(1)$
$dH/dR (\% \cdot \text{min MPa}^{-1}) \times 10^{-3}$	3.8	11.9	60.2

^aNumber in parentheses after the last significant digit is a statistical uncertainty on the $1 - \sigma$ level. ^bCompressibility of WC-8 was estimated using the lattice parameters from Sugiyama et al.⁴⁷ and Santoro et al.²¹ ^cUncertainties of $\frac{1}{v} \cdot \frac{\partial v}{\partial P}$ are propagated uncertainty from the listed lattice parameters.

compressibility is assumed to be similar to that of other silicates and zeolites, where literature values can be found. For this purpose, the lattice parameters of stishovite from Sugiyama et al.⁴⁷ and silicates from Santoro et al.²¹ are used to calculate a mean compressibility value for WC8. The compressibility of ZIF-8 is 1 order of magnitude greater compared to WC8. While the compressibility of $\text{Cu}_2(\text{tebpz})$ is more than double than that of ZIF-8. The calculated compressibility is then related to the dynamic response of the hysteresis to the pressurization rate which is defined as dH/dR . This derivative demonstrates how the intrusion–extrusion hysteresis changes (in %) due to the pressurization rate increase by $1 \text{ MPa}/\text{min}$. The dH/dR was calculated using the data from Figure 3c. It is

demonstrated that for the WC8 and water-system a pressurization rate change of 4 orders of magnitude, ranging from 0.1 MPa min⁻¹ to 1 GPa min⁻¹ increases the hysteresis by approximately 4%. This makes this system attractive for energy dissipation over a wide range of pressurization rates. While, for ZIF-8 and Cu₂(tebpz) a similar increase in pressurization rates results in approximately 10 and 61% hysteresis increase, respectively.

This is shown in Figures 2 and 3. The dependence between the compressibility of a porous material and its hysteresis response is shown in Figure 4, where the dependence between

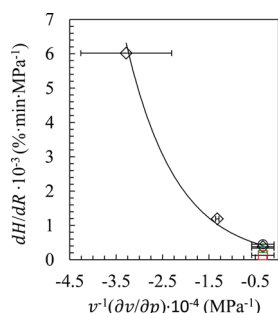


Figure 4. Rate dependence of the water intrusion hysteresis as a function of porous material flexibility. This work (\diamond), MCM-41 (blue \circ) SBA-15 (red \square), and HMS (green \triangle) from Guillemot et al.^{15,16} The error bars represent the confidence interval of 95%.

dH/dR and compressibility is logarithmic. This suggests that the dynamic hysteresis of water intrusion into nanopores can be regulated by the flexibility of a porous material.

The current number of flexible materials which can be used to verify the trend presented in Figure 4 is extremely limited. Moreover, there are only 5 MOFs, which demonstrate water intrusion. Namely, ZIF-8 and Cu₂(tebpz), which are explored in this article. The MOFs ZIF-67^{29,48} and ZIF-7⁴⁰ are unstable and degrade with water during high-pressure intrusion experiments. The last MOF ZIF-71 permits liquid intrusion at a pressure greater than 70 MPa,²⁴ which is too high for high-speed compression/decompression tests with the equipment presented here. In the literature, there are certainly more superhydrophobic porous materials among zeolites and grafted silica. However, they do not provide the required flexibility. To illustrate this point, WC8 is compared to the experimental data taken from Guillemot et al.,^{15,16} of which high-speed compression/decompression cycles were made upon the following grafted silicas: MCM-41, SBA-15, and HMS. All three of these materials have limited flexibility, so their results show similar dynamic hysteretic behavior with the results obtained for WC8. Similar results were obtained for devices designed for an automotive shock-absorber which are based on grafted porous silica and water as described by Eroshenko⁴⁹ and Iwatsubo et al.⁵⁰ They have demonstrated that the dissipation of power, by intrusion–extrusion hysteresis, is almost independent of the compression/decompression speed.

The observed dependence of the dynamic hysteresis on the flexibility of the porous material (Figure 4) can be explained from the perspective of the change in effective pore size upon compression/decompression of the flexible material. For instance, the intrusion pressures can be qualitatively examined using the Laplace equation which represents the intrusion pressures and is defined as $P^{\text{int}} = -2 \gamma \cos\theta r^{-1}$.

Here, the intrusion pressure is represented by the surface tension of the liquid γ , the cosine of the contact angle θ , and the pore size radius r of the materials. The extrusion pressure is best described with a separate phenomenon because they tend to occur below the P^{int} and are dependent on kinetic parameters rather than thermodynamic ones. The liquid extrusion is thus best characterized by bubble nucleation within nanoporous systems,^{34,35} which is also a size-dependent phenomenon. From this simplified approach, it is seen how intrusion–extrusion pressure can change because of effective pore size variation during the compression process. This is particularly visible for Cu₂(tebpz) and water system, see Figure 2c, where rapid pressure increase induces a smaller effective pore size before the intrusion process and results in a higher intrusion pressure. Additionally, the plateau which is originally seen at a pressurization rate of 1 MPa min⁻¹ is now a slope with inflection points, see Figure 2c. From this change in PV behavior, it is seen that during pore filling the solid material is being compressed and further reduces the pore radii. As a consequence, the liquid intrusion pressure rises. Similar behavior is observed with the rate of depressurization. The opposite is observed, for WC8, where a very small change in the $P^{\text{int/ext}}$ values is observed, in Figure 2a, due to its limited compressibility. This insignificant change in the $P^{\text{int/ext}}$ suggests that the pore radii do not change with the increasing rate of pressurization. As seen in Figure 2b, ZIF-8 demonstrates intermediate behavior between WC8 and Cu₂(tebpz).

3.3. Contribution of Nanotriboelectrification to the Dynamic Hysteresis of Water Intrusion.

In the previous article by Grosu et al.,³⁶ it was demonstrated that water intrusion–extrusion into-from the pores of WC8 and ZIF-8 is accompanied by nanotriboelectrification, which contributes to the intrusion–extrusion pressure hysteresis. Therefore, it is necessary to verify that the observed dynamic hysteresis is due to the compressibility of porous materials, rather than rate-dependent nanotriboelectrification. With regards to this, first we tested ZIF-8 for nanotriboelectrification effects during intrusion–extrusion using a high-pressure electric cell (see Section 2.2 and Figure 1). The effects are similar to the previous study³⁶ which are displayed in Figure S8a. While remarkably Cu₂(tebpz) did not demonstrate any nanotriboelectrification effects as seen in Figure S8b. These results show that nanotriboelectrification does not influence the water intrusion pressure hysteresis for Cu₂(tebpz) and explain the nonhysteretic behavior of Cu₂(tebpz) under quasistatic conditions as observed in Figure 2c.

These observations provide crucial insight into the origins of dynamic hysteresis of water intrusion into nanopores. First of all, it suggests that the observed dependence of hysteresis by the rate of pressurization is not due to the nanotriboelectrification phenomenon, but rather due to the flexibility of a porous material. Second, it confirms the initial hypothesis³⁶ that nanotriboelectrification upon nonwetting liquid intrusion/extrusion can occur only under strongly nonequilibrium conditions, allowing the charges along with the double layer separate, which is possible in the cage-like topology of WC8 and ZIF-8. However, in the case of the highly ordered cylindrical pores of Cu₂(tebpz), charge separation is not possible and so no electrification effects are observed.

4. CONCLUSIONS

In this article, the effect of porous materials' flexibility on a dynamic hysteresis of water intrusion was explored for the

benefit of energy storage/dissipation applications. Three superhydrophobic nonporous materials with different flexibility, spanning 1 order of magnitude in compressibility, were used for this purpose. Dynamic compression/decompression cycles with rates spanning 5 orders of magnitude were combined with *in situ* high-pressure vSANS to provide insight into the phenomena. It was demonstrated that the flexibility of a porous material can be efficiently used to exploit the dynamic hysteresis of water intrusion–extrusion. In particular, rate-independent hysteresis was found for rigid grafted silica. While in comparison, the transition from a nonhysteretic molecular spring to shock-absorber behavior was found for the highly flexible Cu₂(tebpz) MOF. ZIF-8 shows intermediate flexibility, which is demonstrated by the intermediate response of hysteresis to changing pressurization rates.

Using a high-pressure electric cell, it was demonstrated that nanotriboelectrification occurs during the intrusion of water into dielectric nanopores. This effect strongly depends on the topology of a porous material. However, this does not have a significant effect on the dynamic hysteresis. In particular, the highly ordered cylindrical pores of Cu₂(tebpz) prevent the double layer separation during the intrusion–extrusion process thus preventing electrification. This is contrary to the observations for the cage-like topology of both WC8 and ZIF-8 during the water intrusion–extrusion process where they both display electrification.

These obtained results open a new niche of application for flexible MOFs. For example, smart pressure-transmitting fluids, capable of dissipating undesirable high-frequency vibrations. By analogy this system works as a mechanical version of the low-pass filter. The advantage of these new suspensions is the possibility to be miniaturized and be adopted to the specific tasks.

■ ASSOCIATED CONTENT

Supporting Information

The Supporting Information is available free of charge on the ACS Publications website at DOI: 10.1021/acsami.9b14031.

Example figures for the high- q region for Cu₂(tebpz) and ZIF-8 and the calculated volume unit cell parameter with their linearly regressed lattice parameters and figures of the electrical cell study for Cu₂(tebpz) and ZIF-8 (PDF)

■ AUTHOR INFORMATION

Corresponding Author

*E-mail: ygrossu@cicenergigune.com..

ORCID

Alexander Lowe: 0000-0002-9700-5873

Mirosław Chorążewski: 0000-0002-8912-9024

Paweł Zajdel: 0000-0003-1220-5866

Dong Luo: 0000-0001-6960-4783

Mian Li: 0000-0003-1293-3636

Dan Li: 0000-0002-4936-4599

Yaroslav Grosu: 0000-0001-6523-1780

Author Contributions

A.L. and M.C. performed transiometry experiments; N.T. and V.S. performed high-speed PV-experiments; M.M., A.L., and S.P. did high-pressure electrification experiments; A.F. and Y.G. performed mercury porosimetry measurements; T.F., D.L., M.L., and D.L. developed, synthesized, and characterized Cu₂(tebpz) MOF; P.Z., J.B.L., and M.B. performed vSANS

experiments; A.L. and Y.G. wrote the paper; Y.G. supervised the work; all the authors discussed and analyzed the data.

Notes

The authors declare no competing financial interest.

■ ACKNOWLEDGMENTS

Access to vSANS was provided by the Center for High Resolution Neutron Scattering, a partnership between the National Institute of Standards and Technology and the National Science Foundation under agreement no. DMR-1508249. PZ acknowledges NIST support within the Guest Researcher program. Certain commercial equipment, instruments, or materials (or suppliers, or software, ...) are identified in this paper to foster understanding. Such identification does not imply recommendation or endorsement by the National Institute of Standards and Technology, nor does it imply that the materials or equipment identified are necessarily the best available for the purpose. The authors (M.C., A.L., P.Z., S.P., and M.M.) would also like to thank Roman Manka head of the technical workshop at the University of Silesia in Katowice as well as the mechanics and machinist for their help. The help of Cristina Luengo with the mercury porosimetry experiments is highly appreciated. We acknowledge the help of Grethe V. Jensen for the help with the Cu₂(tebpz) experiment.

■ ABBREVIATIONS

WC8, mesoporous silica gel SymmetryPrep C8 purchased from WATERS

Cu, copper

tebpz, 3,3',5,5'-tetraethyl-4,4'-bipyrazolate

ZIF, zeolitic imidazolate framework

vSANS, In situ small-angle neutron scattering

■ REFERENCES

- (1) Wolfram, C.; Shelef, O.; Gertler, P. How Will Energy Demand Develop in the Developing World? *J. Econ. Perspect.* **2012**, *26*, 119–138.
- (2) Boldea, I. Electric Generators and Motors: An Overview. *CES-TEMS.* **2017**, *1*, 3–14.
- (3) Fernandes, D.; Pitié, F.; Cáceres, G.; Baeyens, J. Thermal Energy Storage: How Previous Findings Determine Current Research Priorities. *Energy.* **2012**, *39*, 246–257.
- (4) Eroshenko, V. The Unexpected Properties of a Complex Thermodynamical System. *R Acad Sci Ukr SSR Ser. A.* **1990**, *10*, 79–82.
- (5) Eroshenko, V.; Fadeev, A. Intrusion and extrusion of water in hydrophobized porous silica. *Colloid J* **1995**, *57*, 446–449.
- (6) Eroshenko, V.; Fadeev, A. A Study of the Surface of Chemically Modified Porous Silicas by Water Porosimetry. *Zh. Fiz. Khim.* **1996**, *70*, 1482–1486.
- (7) Eroshenko, V. A.; Fadeev, A. Y. Water Porosimetry Technique in Studying of Hydrophobic Porous Solids. *Mendeleev Chem. J.* **1996**, *40*, 116–125.
- (8) Fadeev, A. Y.; Eroshenko, V. A. Study of Penetration of Water into Hydrophobized Porous Silicas. *J. Colloid Interface Sci.* **1997**, *187*, 275–282.
- (9) Eroshenko, V.; Regis, R.-C.; Soulard, M.; Patarin, J. Energetics: A New Field of Applications for Hydrophobic Zeolites. *J. Am. Chem. Soc.* **2001**, *123*, 8129–8130.
- (10) Eroshenko, V.; Regis, R.-C.; Soulard, M.; Patarin, J. Les Systèmes Hétérogènes “Eau–Zéolithe Hydrophobe”: De Nouveaux Ressorts Moléculaires. *C. R. Phys.* **2002**, *3*, 111–119.
- (11) Coiffard, L.; Eroshenko, V. Temperature Effect on Water Intrusion/Expulsion in Grafted Silica Gels. *J. Colloid Interface Sci.* **2006**, *300*, 304–309.

- (12) Coiffard, L.; Eroshenko, V. A.; Grolier, J.-P. E. Thermomechanics of the Variation of Interfaces in Heterogeneous Lyophobic Systems. *AIChE J.* **2005**, *51*, 1246–1257.
- (13) Eroshenko, V. A.; Piatiletov, I.; Coiffard, L.; Stoudenets, V. A. New Paradigm of Mechanical Energy Dissipation. Part 2: Experimental Investigation and Effectiveness of a Novel Car Damper. *Proc. Inst. Mech. Eng., Part D* **2007**, *221*, 301–312.
- (14) Lefevre, B.; Saugey, A.; Barrat, J. L.; Bocquet, L.; Charlaix, E.; Gobin, P. F.; Vigier, G. Intrusion and Extrusion of Water in Hydrophobic Mesopores. *J. Chem. Phys.* **2004**, *120*, 4927–4938.
- (15) Guillemot, L.; Biben, T.; Galarneau, A.; Vigier, G.; Charlaix, E. Activated Drying in Hydrophobic Nanopores and the Line Tension of Water. *Proc. Natl. Acad. Sci. U.S.A.* **2012**, *109*, 19557–19562.
- (16) Guillemot, L.; Galarneau, A.; Vigier, G.; Abensur, T.; Charlaix, E. New Device to Measure Dynamic Intrusion/Extrusion Cycles of Lyophobic Heterogeneous Systems. *Rev. Sci. Instrum.* **2012**, *83*, 105105.
- (17) Gokulakrishnan, N.; Karbowiak, T.; Bellat, J. P.; Vonna, L.; Saada, M.-A.; Paillaud, J. L.; Soulard, M.; Patarin, J.; Parmentier, J. Improved Hydrophobicity of Inorganic–Organic Hybrid Mesoporous Silica with Cage-like Pores. *Colloids Surf., A* **2013**, *421*, 34–43.
- (18) Gokulakrishnan, N.; Parmentier, J.; Trzpit, M.; Vonna, L.; Paillaud, J. L.; Soulard, M. Intrusion/Extrusion of Water Into Organic Grafted SBA-15 Silica Materials for Energy Storage. *J. Nanosci. Nanotechnol.* **2013**, *13*, 2847–2852.
- (19) Han, A.; Kong, X.; Qiao, Y. Pressure Induced Liquid Infiltration in Nanopores. *J. Appl. Phys.* **2006**, *100*, 014308.
- (20) Ryzhikov, A.; Khay, I.; Nouali, H.; Daou, T. J.; Patarin, J. High Pressure Intrusion–Extrusion of Electrolyte Solutions in Aluminosilicate FAU and *BEA-Type Zeolites. *Microporous Mesoporous Mater.* **2016**, *221*, 1–7.
- (21) Santoro, M.; Veremeienko, V.; Polisi, M.; Fantini, R.; Alabarse, F.; Arletti, R.; Quatieri, S.; Svitlyk, V.; van der Lee, A.; Rouquette, J.; Alonso, B.; Di Renzo, F.; Coasne, B.; Haines, J. Insertion and Confinement of H₂O in Hydrophobic Siliceous Zeolites at High Pressure. *J. Phys. Chem. C* **2019**, *123*, 17432–17439.
- (22) Ortiz, G.; Nouali, H.; Marichal, C.; Chaplais, G.; Patarin, J. Energetic Performances of the Metal–Organic Framework ZIF-8 Obtained Using High Pressure Water Intrusion–Extrusion Experiments. *Phys. Chem. Chem. Phys.* **2013**, *15*, 4888–4891.
- (23) Ortiz, G.; Nouali, H.; Marichal, C.; Chaplais, G.; Patarin, J. Versatile Energetic Behavior of ZIF-8 upon High Pressure Intrusion–Extrusion of Aqueous Electrolyte Solutions. *J. Phys. Chem. C* **2014**, *118*, 7321–7328.
- (24) Ortiz, G.; Nouali, H.; Marichal, C.; Chaplais, G.; Patarin, J. Energetic Performances of “ZIF-71 Aqueous Solution” Systems: A Perfect Shock-Absorber with Water. *J. Phys. Chem. C* **2014**, *118*, 21316–21322.
- (25) Khay, I.; Chaplais, G.; Nouali, H.; Marichal, C.; Patarin, J. Water Intrusion–Extrusion Experiments in ZIF-8: Impacts of the Shape and Particle Size on the Energetic Performances. *RSC Adv.* **2015**, *5*, 31514–31518.
- (26) Grosu, Y.; Li, M.; Peng, Y.-L.; Luo, D.; Li, D.; Faik, A.; Nedelec, J.-M.; Grolier, J.-P. A Highly Stable Nonhysteretic {Cu-2(Tebpz) MOF + Water} Molecular Spring. *ChemPhysChem* **2016**, *17*, 3359–3364.
- (27) Sun, Y.; Li, Y.; Tan, J.-C. Framework Flexibility of ZIF-8 under Liquid Intrusion: Discovering Time-Dependent Mechanical Response and Structural Relaxation. *Phys. Chem. Chem. Phys.* **2018**, *20*, 10108–10113.
- (28) Mortada, B.; Chaplais, G.; Veremeienko, V.; Nouali, H.; Marichal, C.; Patarin, J. Energetic Performances of ZIF-8 Derivatives: Impact of the Substitution (Me, Cl, or Br) on Imidazolate Linker. *J. Phys. Chem. C* **2018**, *122*, 3846–3855.
- (29) Grosu, Y.; Gomes, S.; Renaudin, G.; Grolier, J.-P. E.; Eroshenko, V.; Nedelec, J.-M. Stability of Zeolitic Imidazolate Frameworks: Effect of Forced Water Intrusion and Framework Flexibility Dynamics. *RSC Adv.* **2015**, *5*, 89498–89502.
- (30) Grosu, Y.; Eroshenko, V.; Nedelec, J. M.; Grolier, J. P. E. A New Working Mode for Molecular Springs: Water Intrusion Induced by Cooling and Associated Isobaric Heat Capacity Change of a {ZIF-8+water} System. *Phys. Chem. Chem. Phys.* **2015**, *17*, 1572–1574.
- (31) Grosu, Y.; Renaudin, G.; Eroshenko, V.; Nedelec, J.-M.; Grolier, J.-P. E. Synergetic Effect of Temperature and Pressure on Energetic and Structural Characteristics of {ZIF-8+water} Molecular Spring. *Nanoscale* **2015**, *7*, 8803–8810.
- (32) Beurroies, I.; Presle, D.; Rodriguez, J.; Denoyel, R. The Use of Nanoporous Materials for Mechanical Energy Dissipation. In *Poromechanics VI*; 2017; pp 395–402.
- (33) Grosu, Y.; Ievtushenko, O.; Eroshenko, V.; Nedelec, J. M.; Grolier, J. P. E. Water Intrusion/Extrusion in Hydrophobized Mesoporous Silica Gel in a Wide Temperature Range: Capillarity, Bubble Nucleation and Line Tension Effects. *Colloids Surf., A* **2014**, *441*, 549–555.
- (34) Amabili, M.; Grosu, Y.; Giacomello, A.; Meloni, S.; Zaki, A.; Bonilla, F.; Faik, A.; Casciola, C. M. Pore Morphology Determines Spontaneous Liquid Extrusion from Nanopores. *ACS Nano* **2019**, *13*, 1728–1738.
- (35) Tinti, A.; Giacomello, A.; Grosu, Y.; Casciola, C. M. Intrusion and Extrusion of Water in Hydrophobic Nanopores. *Proc. Natl. Acad. Sci. U.S.A.* **2017**, *114*, E10266–E10273.
- (36) Grosu, Y.; Mierzwa, M.; Eroshenko, V. A.; Pawlus, S.; Chorazewski, M.; Nedelec, J.-M.; Grolier, J.-P. E. Mechanical, Thermal, and Electrical Energy Storage in a Single Working Body: Electrification and Thermal Effects upon Pressure-Induced Water Intrusion–Extrusion in Nanoporous Solids. *ACS Appl. Mater. Interfaces* **2017**, *9*, 7044–7049.
- (37) Grosu, Y.; Giacomello, A.; Meloni, S.; González-Fernández, L.; Chorazewski, M.; Geppert-Rybczynska, M.; Faik, A.; Nedelec, J.-M.; Grolier, J.-P. Viscosity at the Nanoscale: Confined Liquid Dynamics and Thermal Effects in Self-Recovering Nanobumpers. *J. Phys. Chem. C* **2018**, *122*, 14248–14256.
- (38) Michelin-Jamois, M.; Picard, C.; Vigier, G.; Charlaix, E. Giant Osmotic Pressure in the Forced Wetting of Hydrophobic Nanopores. *Phys. Rev. Lett.* **2015**, *115*, 036101.
- (39) Soulard, M.; Patarin, J.; Eroshenko, V.; Regis, R. Molecular Spring or Bumper: A New Application for Hydrophobic Zeolitic Materials. In *Studies in Surface Science and Catalysis*; van Steen, E., Claeys, M., Callanan, L. H., Eds.; Recent Advances in the Science and Technology of Zeolites and Related Materials Part B; Elsevier, 2004; Vol. 154, pp 1830–1837.
- (40) Sun, Y.; Li, Y.; Tan, J.-C. Liquid Intrusion into Zeolitic Imidazolate Framework-7 Nanocrystals: Exposing the Roles of Phase Transition and Gate Opening to Enable Energy Absorption Applications. *ACS Appl. Mater. Interfaces* **2018**, *10*, 41831–41838.
- (41) Wang, J.-H.; Li, M.; Li, D. An Exceptionally Stable and Water-Resistant Metal–Organic Framework with Hydrophobic Nanospaces for Extracting Aromatic Pollutants from Water. *Chem.—Eur. J.* **2014**, *20*, 12004–12008.
- (42) Chorazewski, M.; Grzybowski, A.; Paluch, M. The Complex, Non-Monotonic Thermal Response of the Volumetric Space of Simple Liquids. *Phys. Chem. Chem. Phys.* **2014**, *16*, 19900–19908.
- (43) Chorazewski, M.; Grzybowski, A.; Paluch, M. Isobaric Thermal Expansion of Compressed 1,4-Dichlorobutane and 1-Bromo-4-Chlorobutane: Transitionometric Results and a Novel Application of the General Density Scaling-Based Equation of State. *Ind. Eng. Chem. Res.* **2015**, *54*, 6400–6407.
- (44) Haldoupis, E.; Watanabe, T.; Nair, S.; Sholl, D. S. Quantifying Large Effects of Framework Flexibility on Diffusion in MOFs: CH₄ and CO₂ in ZIF-8. *ChemPhysChem* **2012**, *13*, 3449–3452.
- (45) Fairen-Jimenez, D.; Moggach, S. A.; Wharmby, M. T.; Wright, P. A.; Parsons, S.; Duren, T. Opening the Gate: Framework Flexibility in ZIF-8 Explored by Experiments and Simulations. *J. Am. Chem. Soc.* **2011**, *133*, 8900–8902.
- (46) Zhang, K.; Lively, R. P.; Zhang, C.; Chance, R. R.; Koros, W. J.; Sholl, D. S.; Nair, S. Exploring the Framework Hydrophobicity and

Flexibility of ZIF-8: From Biofuel Recovery to Hydrocarbon Separations. *J. Phys. Chem. Lett.* **2013**, *4*, 3618–3622.

(47) Sugiyama, M.; Endo, S.; Koto, K. The Crystal Structure of Stishovite under Pressure up to 6 GPa. *Mineral. J.* **1987**, *13*, 455–466.

(48) Khay, I.; Chaplais, G.; Nouali, H.; Ortiz, G.; Marichal, C.; Patarin, J. Assessment of the Energetic Performances of Various ZIFs with SOD or RHO Topology Using High Pressure Water Intrusion-Extrusion Experiments. *Dalton Trans.* **2016**, *45*, 4392–4400.

(49) Eroshenko, V. Heterogeneous Structure for Accumulating or Dissipating Energy, Methods of Using Such a Structure and Associated Devices. U.S. Patent 6,052,992 A, April 25, 2000.

(50) Iwatsubo, T.; Suciu, C. V.; Ikenagao, M.; Yaguchio, K. Dynamic Characteristics of a New Damping Element Based on Surface Extension Principle in Nanopore. *J. Sound Vib.* **2007**, *308*, 579–590.